I J C T A, 10(5) 2017, pp. 11-20

SEF-DFigure Based Hybrid Grid Connected System

Durga Surya Prakash Chadalwada[*] and R.B.R Prakash[**]

Abstract: Generally, Wind energy systems are in need of the hour from electrical energy system point of view. Doubly fed electric machines are best suited for wind systems due to their ability to work under variable speed conditions in new configuration such as single external feeding of DFigure (SEF-DFIG) which has significant merits over the former system. This paper also proposes the concept of hybrid grid energy system which consists of wind as well as other sustainable energy sources such as PV and FC systems. The performance of this hybrid system is observed by simulation case study demonstrate the usefulness of the proposed system.

Keywords: SEF-DFIG, Solar, Wind, Fuel and Grid System.

1. INTRODUCTION

In the present scenario, maximum utilization of energy demand in the world is based on fossil fuels such as coal, natural gas and petroleum products. But, in this one of the major disadvantage from these products are global warming, and these result in great danger for life on the planet [1].The alternative solution for this fossil fuels are utilization of sustainable energy sources. The power produced by a wind vitality structure relies upon the atmosphere conditions; for example, if in case of rainy or in case of cloudy conditions, it is not possible to meet the energy demand. For flexible and reliable operation of the system, the best solution is to integrate the wind generation system with other renewable sources such as solar, electrolyzer, fuel cell or in some cases grid interconnection.

The capability of fuel cell power generation system, wind energy generation system and photo voltaic based hybrid system can be to overcome the inconvenience caused by the grid power structure. Hence, the coordination of FC, Solar and wind generation system is considered for eliminating the fluctuations [2].

This simulation model is performed using Matlab and Sim Power Systems. To verify the effectiveness of the expected structure results are shown [3]. The proposed grid connected hybrid energy system is described in Figure 1. It explains the structure for hybrid system based fuel cell, solar and wind energy systems. Mechanical power noted from a wind turbine can be given as [6]:

$$P_m = 0.5\rho A C_p V^3$$

The maximum theoretical power coefficient value is 0.59 in the above formula and that value depends upon two different variables i.e. pitch angled tip speed ratio (TSR) and speed of the rotor to the wind speed is TSR linearly. Pitch angle is nothing but the arrangement of turbine blades at an angle with reference to longitudinal axis.

Figure 2 represents the curve of "C Vs. λ" and also the peak value of $C_{p\,\max}$ at λopt is set out. In the practically applicable designs, the largest attainable range for high speed and low speed turbines is 0.4 to 05 and 0.2 to 04 respectively.

[*] PG student, EEE Department, K.L. University, Greenfields, Guntur. *Email: durgasuryaprakash92@gmail.com*

[**] Associate Professor, EEE Department, K.L. University, Greenfields, Guntur. Email: bhanu184@kluniversity.in

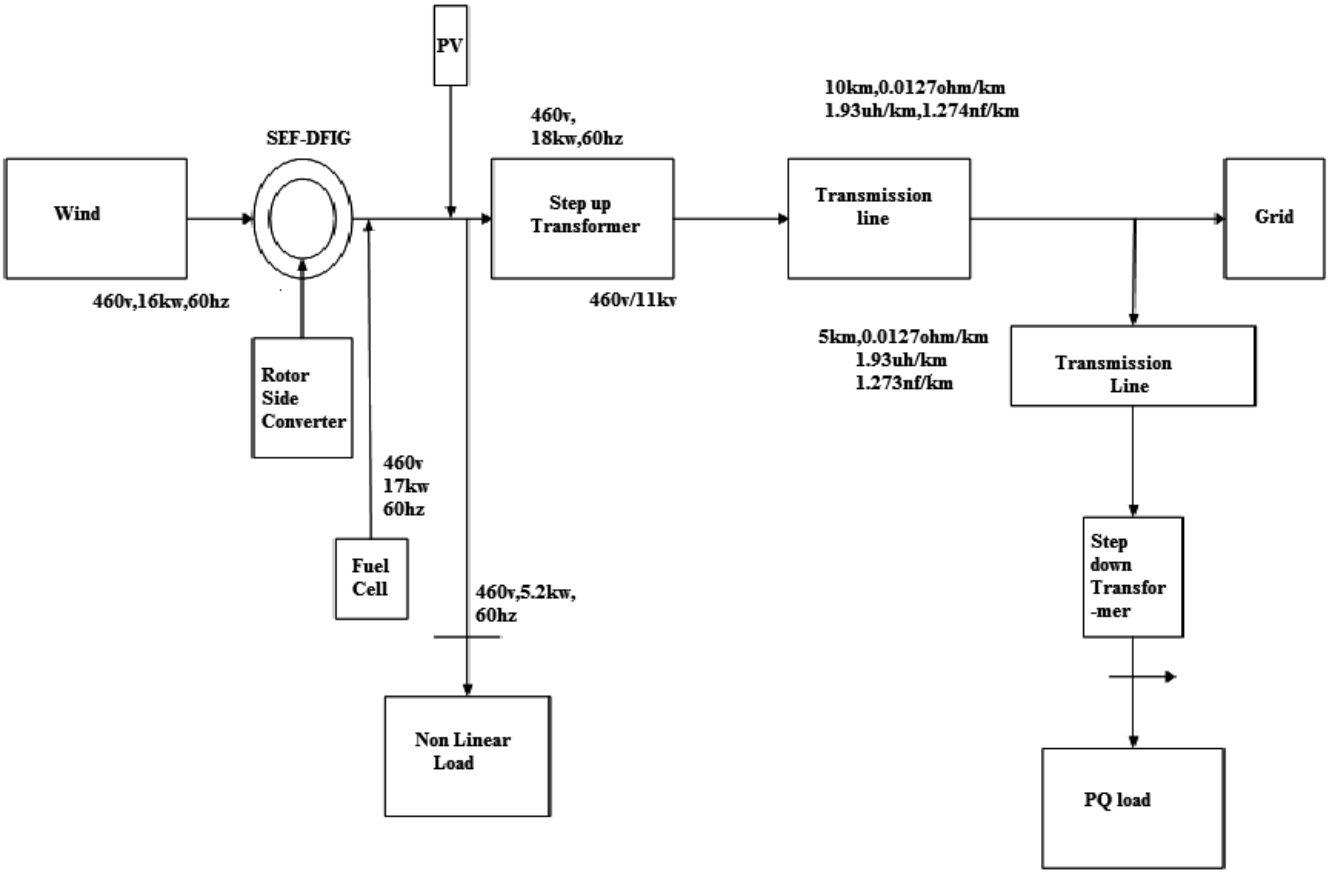

Figure 1: Structure of proposed system

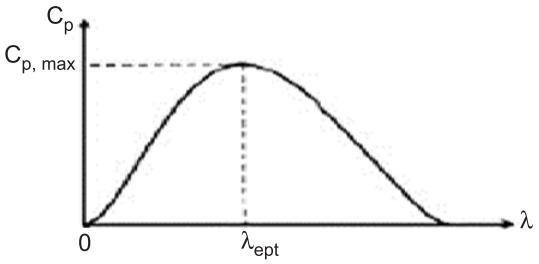

Figure 2: Coefficient of power Vs TSR

For obtaining maximal extent of power from the wind energy generation systems, the mechanical turbine has a potentiality to work at variable speeds and also to conserve the peak power extraction characteristics.

For this, a novel perception in Induction generator is introduced in 1888 acknowledged as Doubly Fed Induction Generator. The DFigure is basically one of the types in wound rotor induction generator which is connected to power system through its stator terminals [4]. The rotor is connected to the power system by means of two back to back converters termed as GSC and RSC. On the other hand, this DFigure has a weakness that it depends upon slip rings and brushes, that gains outfitting as well as maintaince cost.

2. MODELING AND DESIGN OF SEF-DFIG

In order to fulfill the above detailed specifications, a novel configuration in DFigure is intended termed as single external feeding DFigure (SEF-DFIG) in which the RSC converter supersedes the back-back converter in the simple DFIG. This SEF-DFigure accomplishes like a conventional DFIG. As compared with the

DFIG, the SEF-DFigure [5] has the need of only one converter in the rotor side and the consumed power in the inverter is not endowed from the grid. So, by omitting the grid side converter and their correlating filters, it could diminish the system cost and elaboration.

Figure 3 describes the simplified diagram of SEF-DFigure based wind turbine. In this configuration the grid side converter is eliminated. The slip power recovery is maintained by rotor side converter itself. The elimination of grid side converter reduces the system cost and complexity [6].

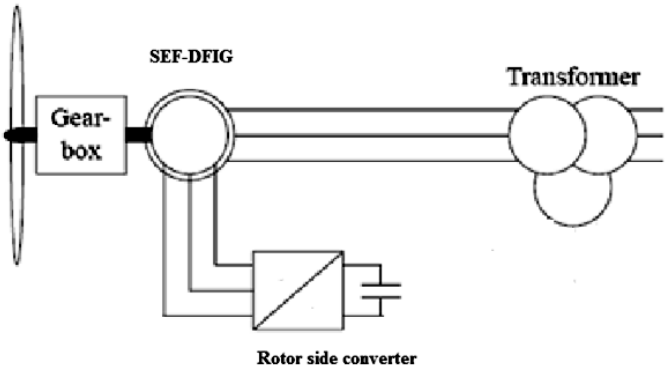

Figure 3: schematic diagram for SEF-DFigure based wind turbine

In the case of $Pr > 0$, there is a reduction in the potential difference levels and also the rotor is given, dc link capacitor stores the energy where as in the case of $Pr<0$, there is rise in potential difference levels and also the dc-link capacitor is fed with the energy from rotor [7].

3. MODELING OF THE SEF-DFIG

Alike the vector control of conventional DFIG, the dc-link voltage control of SEF-DFigure also needs a few extra considerations. In this the power extracted in the RSC inverter flows through rotor windings, the dc-link voltage of RSC converter relays only on the peculiar rotor power P_s [8], retrieved from the rotor windings.

$$\lambda_{ds}^{\omega_e} = \frac{E_g}{\omega_g} \tag{1}$$

$$P_s = -\frac{3}{2}\frac{L_m}{L_s}\omega_e \lambda_{ds}^{\omega_e} I_{qr}^{\omega_e} \tag{2}$$

$$P_s^* = \frac{3}{2}\frac{L_m}{L_s}\omega_e \lambda_{ds}^{\omega_e} I_{qr}^{\omega_e} \tag{3}$$

$$I_{qr}^{\omega_e} = \frac{P_s^*}{\frac{3}{2}\frac{L_m}{L_s}\omega_e \lambda_{ds}^{\omega_e}} \tag{4}$$

$$I_{dr}^{\omega_e} = \frac{\lambda_{ds}^{\omega_e}}{L_m} \tag{5}$$

$$I_{dr,\min}^{\omega_e} = \frac{\lambda_{ds}^{\omega_e}}{L_m} - I_{qr}^{\omega_e}\sqrt{\frac{1-P_{fb}^2}{P_{fb}^2}} \tag{6}$$

$$I_{dr,\,max}^{\omega_e} = \frac{\lambda_{ds}^{\omega_e}}{L_m} + I_{qr}^{\omega_e}\sqrt{\frac{1-P_{fb}^2}{P_{fb}^2}} \tag{7}$$

For vector control of SEF-DFigure and for mathematical analysis, a stator flux reference frame is chosen in SEF-DFigure and the power expression could be written as,

$$P_r = P_{dc} = -V_{dc}I_{dc} \tag{8}$$

Where, V_{dc} is voltage across dc-link capacitor, I_{dc} is the current passing through dc-link capacitor and P_{dc} is the dc-link power. A Proportional Integral controller is designed for controlling rotor power by regulating the dc-link voltage. The reference signals for d-axis current are inherited from the reference of dc-link current.

$$I_{dr}^{\omega_e} = (V_{dc}^{*} - V_{dc})\left(k_p + \frac{k_i}{s}\right) \tag{9}$$

$$k_p = 2c_{dc}\,\zeta\omega_n \tag{10}$$

$$k_i = c_{dc}\,\omega_n^2 \tag{11}$$

$$\lambda_{ds} = V_{ds} - (i_{ds} \times r_s) + (\omega_1 \times \lambda_{qs}) \tag{12}$$

$$\lambda_{ds} = V_{qs} - (i_{qs} \times r_s) + (\omega_1 \times \lambda_{ds}) \tag{13}$$

$$i_{ds} = \frac{\lambda_{ds} - (L_m \times i_{dr})}{L_s} \tag{14}$$

$$i_{qs} = \frac{\lambda_{qs} - (L_m \times i_{qr})}{L_s} \tag{15}$$

$$\lambda_{dr} = V_{dr} - (i_{dr} \times r_r) + (\omega_1 \times \lambda_{qr}) \tag{16}$$

$$\lambda_{qr} = V_{qr} - (i_{qr} \times r_r) + (\omega_1 \times \lambda_{dr}) \tag{17}$$

The power generated in SEF-DFigure is interpreted by I_{qr}. The stableness of the dc link voltage is more momentous. Accordingly, preference for controlling parameter is prone to output of dc link voltage $I_{dr}*$ [9].

$$i_{dr} = \frac{\lambda_{dr} - (L_m \times i_{ds})}{L_r} \tag{18}$$

$$i_{qr} = \frac{\lambda_{qr} - (L_m \times i_{qs})}{L_r} \tag{19}$$

The above mathematical modeling is used for designing of SEF-DFIG. The system parameters for SEF-DFigure are shown in the table.

Table 1
List of Parameters for SEF-DFIG

Element	*Rating*	*Element*	*Rating*
Vdc	200V	Lm	49 mH
Ps	2.4kW	Pfb	0.95
Rs	0.6 ohm	Wg	60 Hz
Rr	0.7 ohm	f	60 Hz
Ls	54 mH	Vrms	220 V
Lr	56 mH	Ts	5e-6

4. SOLAR SYSTEM DESIGN

In the PV network of electrical phenomenon, cell is the necessary part. For the raise in appropriate current, high power and potential difference, the sunlight dependent cells and their region unit joined in non-current or parallel fashion called as PV exhibit are used [9]. In practical applications, each and every cell is similar to diode with the intersection designed by the semiconductor material. When the light weight is absorbed by the electrical marvel sway at the point of intersection, it gives the streams at once.

$$I = I_{ph} - I_D - I_{sh} \tag{20}$$

$$I = I_{ph} - I_o\,[\exp(qV_D/nKT)] - (v_D/R_S) \tag{21}$$

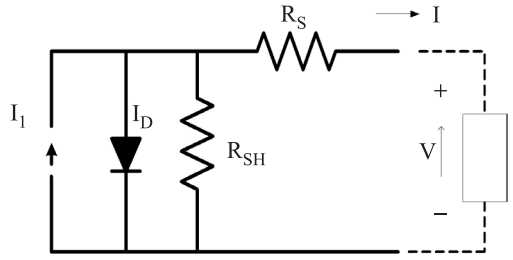

Figure 4: PV Electrical Equivalent circuit

Solar cell output power is given as the product of V and I

The (current-voltage) and (Power-Voltage) attributes at absolutely unpredictable star intensities of the PV exhibit [10] are represented in Figure 3, whereas the often seen existence of most electrical outlet on each yield is shown in power diagram 4.

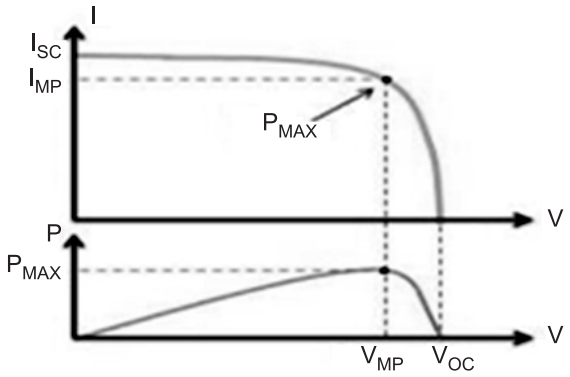

Figure 5: Response of output characteristics of PV Array

5. DESIGN OF FUEL CELL

The H_2 molecules are brought by the anode side flow plate channels during the beginning of electro chemical procedure for the fuel cells. Over an external electrical circuit [11], the electro stat transits to cathode while the proton travels to cathode through a membrane in which the anode catalyst separates H_2 on protons H^+. For the development of Heat and water, O_2 is associated with electrons and H_2 proton at the cathode by using a catalyst. This entire process is represented in below equations [12].

$$H_2 \rightarrow H_2O + 2e^-(\text{Anode}) \tag{22}$$

$$\frac{1}{2}O_2 + 2H^+ + 2e^- \rightarrow H_2O(\text{Cathode}) \tag{23}$$

$$\Delta g_g = \Delta g_f^o - \mathrm{R}T_{fc}[\ln(\mathrm{PH}_2) + 0.5\ln(\mathrm{PO}_2)] \tag{24}$$

The free energy, at basic standard Gibbs pressure is represented as Δg^o_f, T_{fc} PEM temperature and p_{O2},R is the universal gas constant and PH_2 is gas pressure [13]. The equation for the electrical work performed by the fuel cell system with reference to the releasing of chemical energy is

$$\mathrm{E} = -\left(\frac{\Delta_{gf}}{2\mathrm{F}}\right) \tag{25}$$

Through the membrane of H_2 proton mitigation, the parasitic electro chemical reactions [14] are formed at zero currents while on the other hand, due to the cathode and anode activation losses, the electro-proton chemical bonds association and breaking are obtained.

Potential drop of the fuel cell is represented as

$$\mathrm{V}_{\mathrm{act}} = \mathrm{V}_0 + \mathrm{V}_a(1 - e^{-\mathrm{C}_1 i}) \tag{26}$$

The potential difference at zero current density v_0 relies on pressure of cathode and saturation of water, $V_a = f(T_{fc}, P_{ca}, P_{sat})$drop in potential V_a is included in the above expression interrelated with the current density as $V_a = f(T_{fc}, P_{o2}, P_{sat})$ [15]-[16] and whereas the activation voltage constant is c_1 and these are entirely established according to the fuel cell temperature.

6. ELECTRIC CIRCUIT OF FC SYSTEM

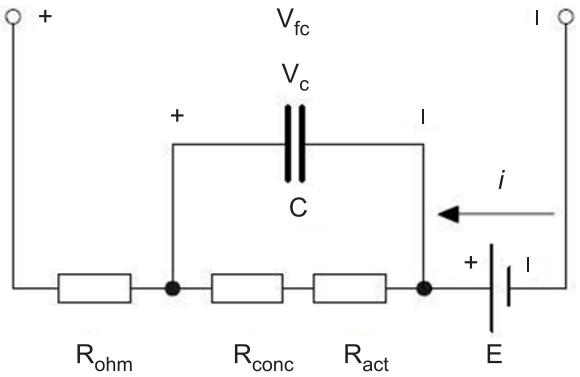

Figure 6: Equivalent circuit for fuel cell system

$$\mathrm{V}_{\mathrm{fc}} = \mathrm{E} - \mathrm{V}_c - \mathrm{IR}_{\mathrm{ohm}} \tag{27}$$

$$\mathrm{C}\frac{d\mathrm{V}_c}{dt} + \frac{\mathrm{V}_c}{\mathrm{R}_{\mathrm{act}} + \mathrm{R}_{\mathrm{conc}}} = i \tag{28}$$

$$\mathrm{V}_{\mathrm{fc}} = \mathrm{E} - \left(\frac{\mathrm{R}_{\mathrm{act}} + \mathrm{R}_{\mathrm{conc}}}{sc(\mathrm{R}_{\mathrm{act}} + \mathrm{R}_{\mathrm{conc}} + 1)} + \mathrm{R}_{\mathrm{ohm}}\right) i \tag{29}$$

7. RESULT AND DISCUSSION

The proposed hybrid model is simulated and tested under different conditions like change in wind speed, solar irradiation changes and also at different loads. The dc link voltage is sustained constant by the controller irrespective of these changes. This proposed system is experimentally verified by using Matlab/Simulation and the consummation of the system is distinguished by the preceeding waveforms.

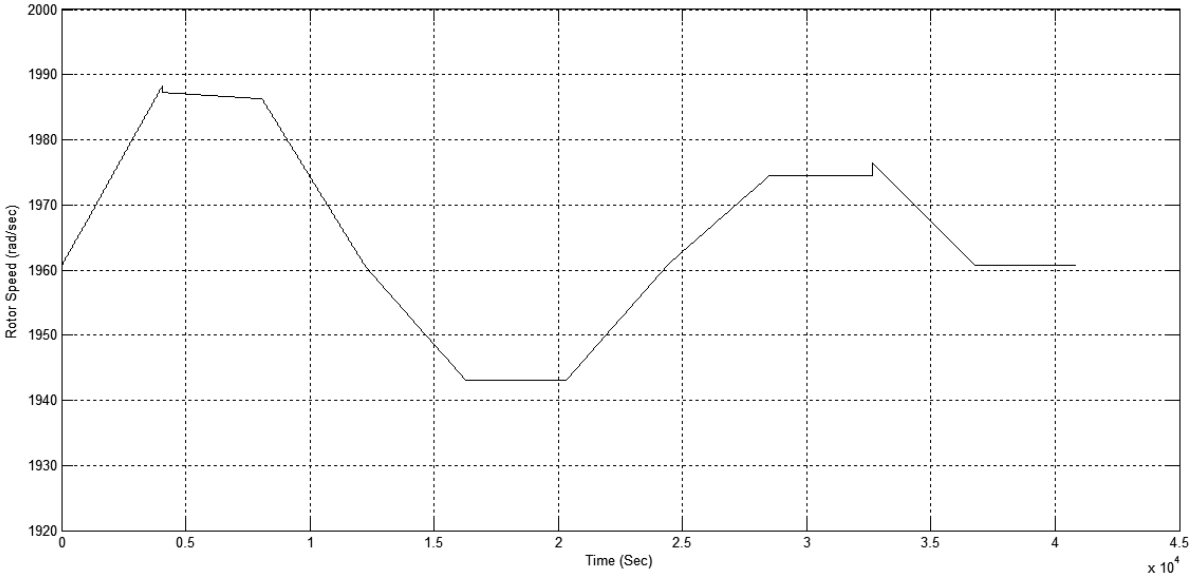

Figure 7: Speed vs time of SEF-DFIG

Figure 7 explains the simulation result for wind turbine speed and it is chosen based on time to time variation. Figure 8 shows the simulation result for three phase voltage and current from the SEF-DFigure structure. Figure 9 is the simulation result for active and reactive powers at grid terminals.

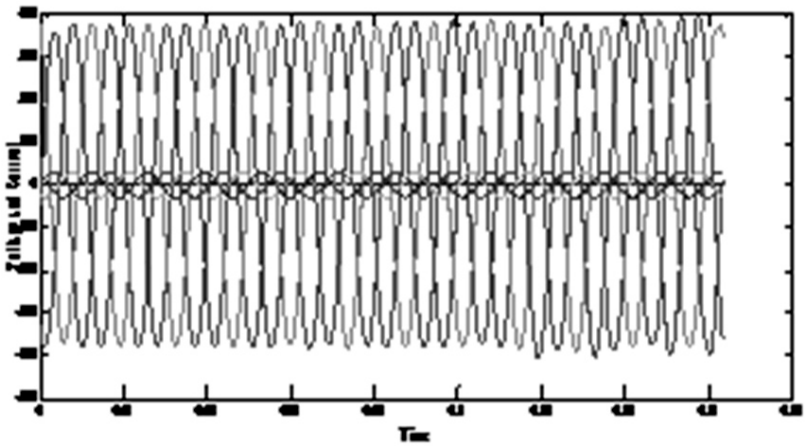

Figure 8: Voltage and Current vs time of SEF-DFIG

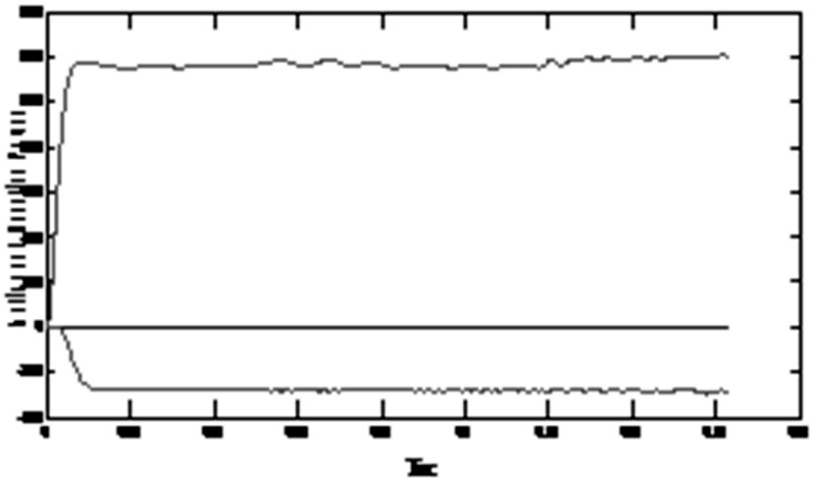

Figure 9: P&Q vs time of SEF-DFIG

Figure 10 and Figure 11 are the simulation results which shows the active and reactive powers for grid connected hybrid energy system.

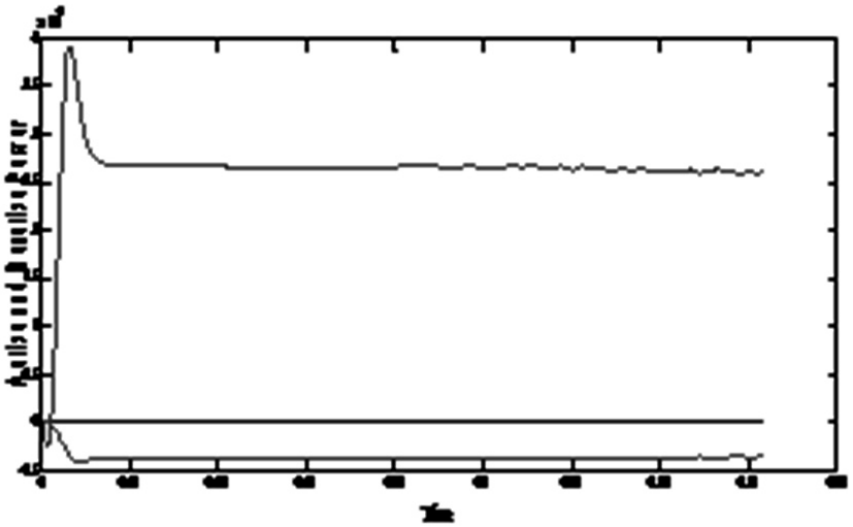

Figure 10: P&Q at the grid terminals when all the sources are connected

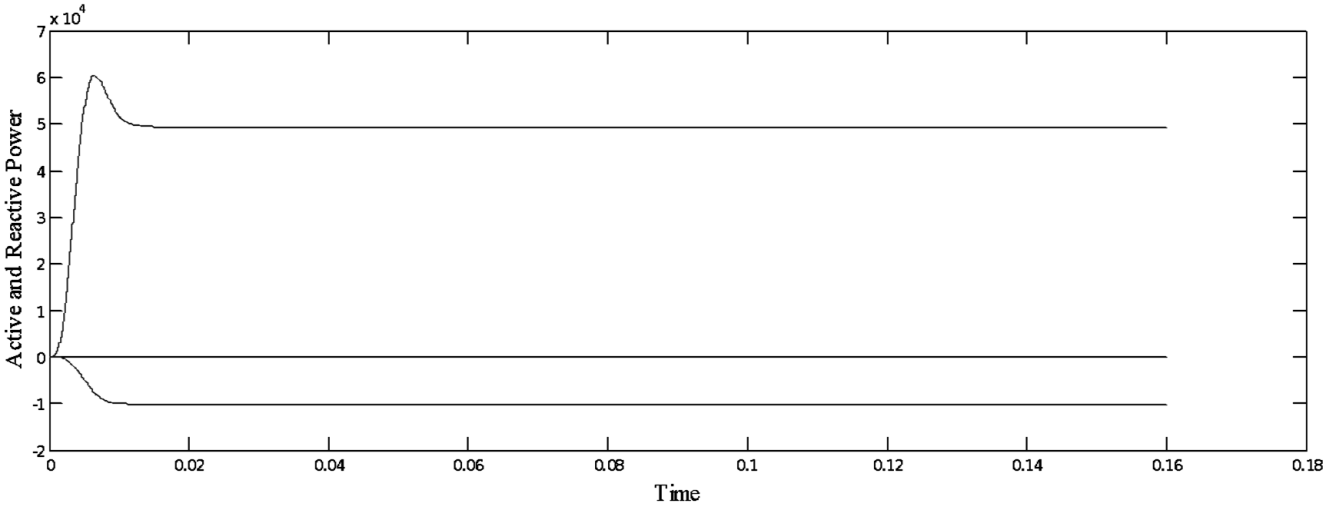

Figure 11: Simulation Result for active and reactive power at Load terminals

Table 2
Real and reactive power consumption in the proposed hybrid grid connected system

MODE OF OPERATION	*WIND*		*PV*		*FUEL CELL*		*GRID*		*LOAD*	
	P	*Q*	*P*	*Q*	*P*	*Q*	*P*	*Q*	*P*	*Q*
W + P + F	11.6k	2.9k	6.4k	2.3k	9.5k	2.5k	28.7k	5.5k	55.2k	13k
W + F	11.6k	2.9k	–	–	9.5k	2.5k	34k	7.5k	55.2k	13k
W + P	11.6k	2.9k	6.4k	2.3k	–	–	37.2k	7.9k	55.2k	13k
P + F	–	–	6.4k	2.3k	9.5k	2.5k	39k	8.2k	55.2k	13k
W	11.6k	2.9k	–	–	–	–	43.2k	9.7k	55.2k	13k
P	–	–	6.4k	2.3k	–	–	48.8k	10.6k	55.2k	13k
F	–	–	–	–	9.5k	2.5k	45.5k	10.5k	55.2k	13k

For better supervision the modes of operation and power flow management in power system a supervisory controller is used. In this paper, load management is main constraint and performed for increasing the

independence of hybrid system towards the utility grid. In this paper is load is designed for rating of 55.2 kW and 13 Mvar. For meeting this load demand this proposed system implemented under different cases along with utility grid. For example if only wind and solar is kept in active state and fuel cell is in shut down condition. Depend on the input conditions only 21.1 KW and 5.5 Kvar is generated from the hybrid system and the remaining power is extracted from the grid. The table shown above shows the load demand requirement from hybrid based grid system under different cases.

The main constraint for ay hybrid system is to decrease the cost of the system. For this, general calculations have been done in order to simulate those conditions for long term analysis of grid system. Since the potential of solar region is more than the wind generation capacity. Power generation is contributed at lower cost with PV system and the utilization of wind system is the more cost effective solution. In addition, a Fuel Cell system is taken into consideration along with solar and wind energy systems in the optimum configuration in the case of raise in grid electricity price.

Nevertheless, if the allowed capacity shortage is raised more, then the optimized hybrid system is regarded as solar, wind and grid connection. More increase in capacity shortage reduces the energy storage, which leads to usage of fuel cell energy system in this hybrid system. However, dependence on the changes in capital shortage the optimized hybrid system can be calculated, respectively as grid-solar, grid-wind, grid-wind-solar, grid-wind-solar, grid-wind-solar-fuel cell and grid-wind-solar-fuel cell which depends on the electricity rate changes.

8. CONCLUSION

The effectiveness of isolated power systems are evaluated in MATLAB PC environment. The system considered is wind along with PV and fuel cells to meet the load which is highly advantageous for remote and inaccessible loads. The proposed DFigure configuration is better compared to the conventional configuration with more power output and improved system characteristics. It is observed that the proposed configuration is low cost and having less complexity. The gird is utilized to supply to the unmet power demand by the isolated power systems if they are connected to the gird. On the whole, the performance of isolated system is better and economically beneficial to the customers at large and is very effective for rural areas to meet remote loads.

References

1. R. Datta and V. T. Ranganathan, "Variable-speed wind power generation using doubly fed wound rotor induction machine—A comparison with alternative schemes," *IEEE Trans. Energy Convers., Vol. 17, No. 3, pp. 414–421, Sep. 2002.*
2. J. Arbi, M. J.-B. Ghorbal, I. Slama-Belkhodja, and L. Charaabi, "Direct virtual torque control for doubly fed induction generator grid connection," *IEEE Trans. Ind. Appl., Vol. 47, No. 1, pp. 4163–4173, Jan./Feb. 2011.*
3. A. Luna, K. Lima, D. Santos, R. Paul, and S. Arnaltes, "Simplified modeling of a DFigure for transient studies in wind power applications," *IEEE Trans. Ind. Electron., Vol. 58, No. 1, pp. 9–19, Jan 2011.*
4. M. J. Hossain, H. P. Pota, V. A. Ugrinovskii, and R. A. Ramos, "Simultaneous STATCOM and pitch angle control for improved LVRT capability of fixed-speed wind turbines," *IEEE Trans. Sustainable Energy, Vol. 1, No. 3, pp. 142–151, Oct. 2010.*
5. A. Cause brook, D. J. Atkinson, and A. G. Jack, "Fault ride-through of large wind farms using series dynamic braking resistors," *IEEE Trans. Power Syst., Vol. 22, No. 3, pp. 966–975, Aug. 2007.*
6. M. E. Haque, M. Negnevitsky, and K. M. Muttaqi, "A novel control strategy for a variable-speed wind turbine with a permanent-magnet synchronous generator," *IEEE Trans. Ind. Appl., Vol. 46, No. 1, pp. 331–339, Jan./Feb 2010.*
7. W. Oiao, L. Qu, and R. G. Harley, "Control of IPM synchronous generator for maximum wind power generation considering magnetic saturation," *IEEE Trans. Ind. Appl., Vol. 45, No. 3, pp. 1095–1105, May/Jun. 2009.*
8. C. S. Brune, R. Spee, and K. Wallace, "Experimental evaluation of a ´ variable-speed doubly-fed wind-power generation system," *IEEE Trans. Ind. Appl., Vol. 30, No. 3, pp. 648–655, May/Jun. 1994.*

9. S. Bhowmik, R. Spee, and J. H. R. Enslin, "Performance optimization ´ for doubly fed wind power generation systems," *IEEE Trans. Ind. Appl., Vol. 35, No. 4, pp. 949–958, Jul/Aug. 1999.*

10. C.-H. Liu and Y.-Y. Hsu, "Effect of rotor excitation voltage on steady-state stability and maximum output power of a doubly fed induction generator," *IEEE Trans. Ind. Electron., Vol. 58, No. 4, pp. 1096–1109, Apr. 2011.*

11. A. Petersson and S. Lundberg, "Energy efficiency comparison of electrical systems for wind turbines," in Proc. *IEEE Nordic Workshop Power Ind. Electron. (NORPIE), Stockholm, Sweden, Aug. 2002, pp. 12–14.*

12. C. Smith, R. Todd, M. Barnes, and P. J. Tavner, "Improved energy conversion for doubly fed wind generators," *IEEE Trans. Ind. Appl., Vol. 42, No. 6, pp. 1421–1428, Nov./Dec. 2006.*

13. S. Muller, M. Deicke, and R. W. De Doncker, "Doubly fed induction ¨ generator systems for wind turbines," *IEEE Ind. Appl. Mag., Vol. 8, No. 3, pp. 26–33, May/Jun. 2002.*

14. G. D. Marques and D. M. Sousa, "Air-gap-power-vector-based sensor less method for DFigure control without flux estimator," *IEEE Trans. Ind. Electron., Vol. 58, No. 10, pp. 4717–4726, Oct. 2011.*

15. A. Petersson, L. Harnefors, and T. Thiringer, "Evaluation of current control methods for wind turbines using doubly-fed induction machine," *IEEE Trans. Power Electron., Vol. 20, No. 1, pp. 227–235, Jan. 2005.*

16. L. Gao, B. Guan, Y. Zhou, and L. Xu, "Model reference adaptive system observer based sensor less control of doubly-fed induction machine," in *Proc. 2010 Int. Conf. Electrical. Mach. Syst., Oct. 2010, pp. 931–936.*